Synergy achieved in silver-TiO_2 nanocomposites for the inhibition of biopatina on limestone

J. Becerra[1,*], A.P. Zaderenko[1], M.J. Sayagués[2], R. Ortiz[1], P. Ortiz[1]

[1] Departamento de Sistemas Físicos, Químicos y Naturales, Universidad Pablo de Olavide, ES-41013 Seville, Spain.

[2] Instituto de Ciencia de Materiales de Sevilla (CSIC-US), ES-41092-Seville, Spain.

[*]Corresponding author: J. Becerra: jbeclun@upo.es

Abstract

Biodeterioration of stone monuments is estimated to be as high as 20-30% of the total degradation suffered by Cultural Heritage constructions. With regard to this problem, bactericidal treatments are mainly based on cleaning. These processes, while effective in the short term, require frequent reapplications increasing potential damages to the monument. Silver nanoparticles offer many advantages over traditionally employed products, such as their prolonged biocide efficacy and their low toxicity to humans and environment. The aim of this study was to evaluate the applicability and effectiveness of seven nanocomposite treatments based on titanium dioxide and/or silver nanoparticles to prevent biodeterioration of limestone monuments. These nanocomposites were characterized by UV-Visible spectrophotometry, Dynamic Light Scattering and Electron Microscopy. To assess their bactericidal activity, accelerated weathering tests were performed on limestones from the quarry of Utrera, a source widely employed in such iconic monuments as the Cathedral of Seville (Spain). Furthermore, the samples of biopatina employed in our assays stemmed from the façades of historical buildings from Seville. Our results show that silver and titanium dioxide nanocomposites stabilized by citrate achieve a high biocide effect while maintaining color alterations at a low level.

Keywords

Biopatina, biocide, limestone, conservation and restoration, silver-titanium dioxide nanocomposite, stone biodeterioration

1. Introduction

Biodeterioration of stone monuments and archaeological remains is an undesirable change caused by biological agents, whose impact is estimated at around 20-30% of the total degradation suffered by Cultural Heritage constructions [1]. Biological agents involved in biodeterioration include a wide variety of organisms and microorganisms. Bacteria and algae are the most common life forms dwelling on stone buildings, favoring the appearance of biopatina over the stone surface. These biopatinas act through physical and chemical processes. Physical processes are related to the adhesion systems of the microorganisms on the stone substrate, generating chromatic changes, while chemical processes imply reactions that transform or break down the stone substrate causing disintegration and crumbling. In the case of microorganisms, chemical processes are associated with their metabolism as they can disaggregate carbonate stones due to the generation of organic acids. Bacteria are involved in significant chemical processes that vary according to their feeding. Autotrophic bacteria are characterized by inducing solubilisation processes that include acidification of the medium and eating away the stone structure, while the adverse effects of heterotrophic bacteria are mainly due to the production of chelating substances and organic and inorganic acids and alkalis. Nevertheless, in both types of bacteria the main alterations observed are brown and black patinas and exfoliation [2].

Algae and cyanobacteria are often the first microorganisms to colonize the stone surface [3]. For that, specific environmental conditions are necessary such as intense light, high humidity or water, high temperature and alkaline pH. Patinas and crusts of different colors are the principal alterations loosely attributed to weathering [4] which depend on factors like amount of light, available nutrients, temperature, colony aging, etc...[1]. Furthermore, these patinas favor the build-up of dust, spores, other organic compounds, etc, that constitute a special dwelling ground for other biological colonizers (lichens, fungi and vascular plants) [5], and they maintain high moisture levels due to mucilaginous pods.

The absolute cost caused by biodeterioration is difficult to quantify [2], and the cost of cleaning, restoration and maintenance is increasing owing to the increase of detrimental external factors, such as pollution. Some limestones widely employed in the construction of historical buildings [6], are colonized by microorganisms owing to their porous nature. This microbiological colonization,

54 which takes place especially in dark and damp areas of buildings built with this material, leads to the
55 development of biopatina and biocrust that constitute a fertile substrate for higher order plants.
56 Besides favoring colonization by plants, microorganisms are a major cause of deterioration by
57 themselves, as biopatina and biocrust not only produce undesirable alterations of the appearance of the
58 material, but they can also produce fractures and loss of material, as mentioned above. Figure 1 shows
59 representative images of biopatina and biocrust growth on limestone surfaces from monuments in
60 southern Spain.

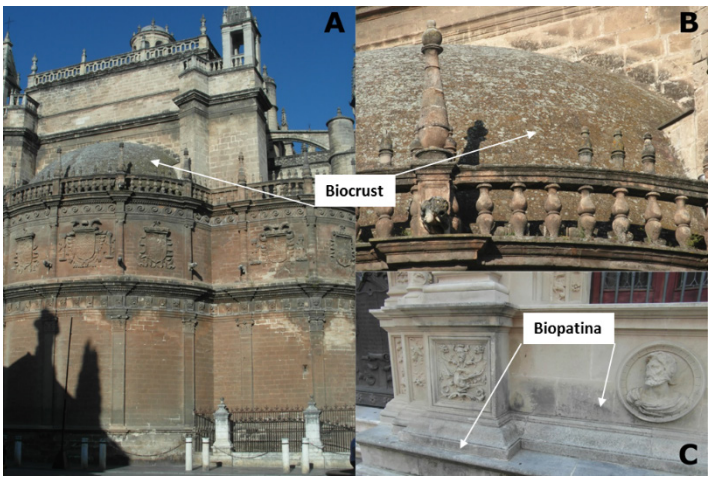

61

62 **Fig. 1.** General (A) and expanded (B) views of biocrust in the vaults of the Cathedral of Seville. New onset of
63 biopatina in the main façade of the City Hall of Seville (C) one year after its restoration.

64 Current bactericidal treatments are mainly based on cleaning. These cleaning processes, while
65 effective in the short term, require frequent reapplications which also increase potentially the damage
66 to the monument. Different treatments are currently employed to prevent the appearance and growth
67 of these alteration agents and their effects on buildings. Most of them are chemical methods like
68 tributyltin, phenolic compounds, quaternary ammonium compounds, etc. These methods have
69 important disadvantages, however, like their high toxicity to humans and environment, their short-
70 lasting effects and possible incompatibility with the substrate stone. For example, limestones are
71 highly sensitive to acid action involved in most treatments, or the color changes caused by tributyltin
72 on travertine stones [7]. Bastian et al. [8] highlighted that these treatments can cause irreversible
73 changes in the original materials, and have even favored the appearance of new microorganisms. New
74 treatments based on silver nanoparticles (AgNPs) with biocide effects bear the promise to avoid these
75 disadvantages [9,10] which is endorsed by the good results obtained in other disciplines such as

medicine, cosmetics, textile industry or environmental remediation [11]. There are several explanations for the interaction of AgNPs with microorganisms, although the precise mechanism is not yet well understood [12]. It is a multifactorial process in which the cellular wall and the plasma membrane of the bacteria are damaged, and so is the inhibition of the protein synthesis and DNA replication [13–15]. These effects are due to the slow release of Ag^+ ions over time in the case of some nanoparticles that favors their long-term biocide effects at lower concentrations than silver salts.

AgNPs biocide properties have been confirmed in different microorganisms, among them, Gram-negative bacteria (*Escherichia coli, Pseudomonas aeruginosa* and *Acinetobacter baumannii*) and Gram-positive bacteria (*Staphylococcus aureus, Enterococcus faecalis, Candida albicans* and *Listeria monocytogenes*) [12–15]. Notably, biocide activity was related to nanoparticle size [14], shape [16] or reducing agent employed in their synthesis [17]. The main advantages offered over traditionally employed products are their prolonged biocide efficacy against a wide variety of microorganisms and their low toxicity to humans and environment [10,18].

On the other hand, titanium dioxide nanoparticles (TiO_2NPs) are one of the most versatile nanoparticles used in construction and building materials due to their stability over time, their compatibility with traditional materials and their high photocatalytic activity which makes them suitable for self-cleaning surfaces [19–21]. This last property, together with hydrophilic properties in presence of UV radiation [20,22], allows to generate a protecting film against deposits from environmental pollution. TiO_2NPs decompose both organic and inorganic substances that cause staining and degradation of stone walls [20,21]. The durability of treatments and their inalterability have been studied too [19,23,24], as well as the mechanism for their biocide properties. As biocide, TiO_2NPs cause oxidation in the microorganism cell walls and hinder or at least interfere with their respiration [25,26], especially under UV radiation.

The use of combined silver and titanium dioxide into a single nanocomposite (Ag/TiO_2) seeks to complement and improve the specific properties on construction materials that these nanoparticles exhibit separately. The presence of silver on the surface of TiO_2NPs increases its chemical reactivity under visible light, so its catalytic activity is not dependent on the availability of UV radiation [27,28]. The biocide effects of Ag/TiO_2 nanocomposites have been checked for other applications against

104 several species of bacteria (*Pseudomonas stutzeri, Stenotrophomonas maltophilia, Micrococcus luteus,*
105 *Bacillus subtilis, Staphylococcus aureus, Escherichia coli, Klebsiella pneumonia* and *Pseudomonas*
106 *aeruginosa* [27,29,30]) and fungi (*Candida albicans* [29,30]). The structure of this kind of
107 nanocomposite is a silver shell around a TiO_2 core; although the inverse structure, TiO_2 shell around a
108 silver core, has been investigated too, and both configurations were shown to be efficient as biocides
109 [31–33]. La Russa et al. [27] have made a first approach confirming the biocide effectiveness of
110 Ag/TiO_2 nanocomposites in a diffusion test on agar plates that extrapolates to stone protection.
111 Nevertheless, inhibition of biopatina formation on stone has not been demonstrated until now. In a
112 study by Bellissima et al. [9], although they applied AgNPs functionalized with tetraethylorthosilicate
113 (TEOS) on stone, they do not measure the biopatina inhibition faculty of these nanoparticles, only
114 their effectiveness as an antibacterial treatment.

115 In this paper, the applicability of Ag/TiO_2 nanocomposites to inhibit biopatinas on stone
116 façades and walls has been studied, checking their biocide properties to determine their effectiveness
117 and applicability under real-world conditions. Remarkably, the samples of biopatina employed in our
118 assays stemmed from the façades of historical buildings.

119 2. Materials and methods

120 *2.1. Stone sampling*

121 Due to the abundance of quarries of carbonate stone in western Andalusia, this type of stone
122 has been widely used as building material in this region since ancient times. Our study focuses
123 specifically on a representative limestone from one of the main suppliers, the quarry of Utrera (Seville,
124 Spain). Remarkably, this limestone has been employed in the construction of some of the most iconic
125 historic buildings in southern Spain, such as the Cathedral or the Town Hall in Seville [34,35], so it is
126 considered one of the most important quarries in southern Spain.

127 Limestone from the quarry of Utrera is a carbonated bioclastic limestone with a high content
128 of quartz and fossils (2-5%) [34] and a high open porosity (10 %) [36] with pore sizes of 0.1-1 μm
129 [34]. Additionally, the high content and widespread distribution of fossil material generates an intra-

130 porosity that is not connected. The samples used in this study have a size of 1.5 x 1.5 x 0.5 cm.

131 *2.2. Synthesis of silver nanoparticles and silver/titanium dioxide nanocomposites*

132 Silver nitrate ($AgNO_3$) and trisodium citrate were purchased from Panreac, titanium dioxide
133 (P25) from DEGUSSA and sodium borohydride ($NaBH_4$) from Sigma-Aldrich. All other chemicals
134 were reagent grade. Water was purified using a Milli-Q reagent grade water system from Millipore.

135 Silver nanoparticles stabilized by citrate (Ag@cit) were synthesized according to the method
136 described by Flores *et al* [37]. Briefly, an aqueous solution of $AgNO_3$ (1 mL, 0.005 mmol) was added
137 to an aqueous solution of trisodium citrate (16 mL, 0.169 mmol) under magnetic stirring in an ice bath.
138 Thereafter, 100 µL of an aqueous solution of $NaBH_4$ (0.01 mmol) were added dropwise and the
139 reaction mixture was stirred for 1 h and 45 min. The resulting pale yellow aqueous-colloidal
140 suspension of Ag@cit nanoparticles was kept in darkness until its use in biocide assays. This protocol
141 was adapted to obtain two silver/TiO_2 nanocomposites, Ag@cit /TiO_2 and 2xAg@cit/TiO_2, with molar
142 ratios of Ag:TiO_2 of 0.04 and 0.08, respectively, by adding proper amounts of TiO_2 to the initial
143 $AgNO_3$ aqueous solution before the reduction reaction.

144 In addition to the citrate-stabilized nanocomposites, three nanocomposites based on naked
145 silver (i.e., without adding citrate as stabilizing agent during the synthesis of the silver nanoparticles)
146 were prepared. Briefly, an aqueous solution of $NaBH_4$ (4 mL, 0.04 mmol) was added drop by drop to
147 20 mL of an aqueous solution of $AgNO_3$ (0.02, 0.01 or 0.005 mmol) and TiO_2 (0.12 mmol) under
148 magnetic stirring in an ice bath. The reaction mixture was stirred for 10 min. Depending on the
149 amount of silver used in the synthesis three different nanocomposites were obtained: Ag/TiO_2,
150 2xAg/TiO_2 and 4xAg/TiO_2, with molar ratios of Ag:TiO_2 of 0.04, 0.08 and 0.16, respectively. The
151 resulting pale yellow aqueous-colloidal suspensions of naked-silver/TiO_2 nanocomposites were kept in
152 darkness until being used in biocide assays.

153 All the obtained nanoparticles and nanocomposites have been characterized by UV-Visible
154 (UV-Vis) spectrophotometry and Dynamic Light Scattering (DLS). UV-Vis spectra were recorded on
155 an Ocean optics spectrometer equipped with a HR4000 detector (Dunedin, FL. USA). Hydrodynamic
156 diameter (HD) and zeta potential (ζ) were determined by DLS on a Zetatrac Analyzer (Microtrac,

157 USA). Measurements were carried out at 25 °C in water, by placing proper amounts of the
158 nanocomposite suspensions in the sample holders. The morphology and structure of the Ag@cit/TiO_2
159 nanocomposite at the microscopic level were analyzed using Scanning Electron Microscopy (SEM)
160 and Transmission Electron Microscopy (TEM). SEM images were recorded in a GeminiSEM 300
161 microscope. For TEM experiments we employed a high resolution TEM with field mission gun (FEG-
162 HRTEM) from FEI Company (TECNAI G2 F30 S-twin), with a Fischione high angle annular dark-
163 field detector (HAADF) (0.16 nm point resolution) to work in Scanning Transmission Electron
164 Microscopy (STEM) mode, and one INBCA ZX-max 80 silicon drift detector for Energy-dispersive
165 X-ray spectroscopy (EDXS) analysis. The experiments were performed at 300 kV with a resolution of
166 0.2 nm. The analysis of HR micrographs and the Fast Fourier transform (FFT) for phase interpretation
167 were performed with Digital Micrograph software (Gatan Inc.) and the Java version of JEM Software.
168 The analysis of the HAADF-STEM images and the EDS spectra profile were done with ES Vision
169 software (FEI Company). The samples for the microcharacterization of both composites were prepared
170 by drying a drop of the suspensions on a carbon coated copper grid.

171 *2.3. Biopatina sampling and characterization*

172 The vulnerability of historical buildings to different agents in Seville was previously studied
173 by some of the authors of this work in the façades of thirty monuments from this city [38]. In the
174 present study we have evaluated the frequency and degree of biodegradation of these façades and the
175 necessity of a preventive conservation treatment based on biocides. The biodegradation levels were
176 classified according to the *Vulnerability Index* described by Ortiz and Ortiz [39] as follows: low
177 frequency, which indicates that the presence of the biodegradation is incipient and still difficult to
178 detect; medium frequency, which indicates that weathering forms are easily identified, and high
179 frequency, which indicates a high rate of occurrence.

180 To design the accelerated weathering test we used real-life algae grown on monuments
181 affected by biodeterioration. Thirteen samples of biocrust from the façades were cut out with a scalpel
182 and studied by scanning electron microscopy (SEM-EDX JEOL JSM-5400), X-ray diffraction (XRD
183 Bruker D8C) and Zarbeco handheld digital microscope. Afterwards, the samples of biocrust were

cultured in a phosphate-rich medium ($NaH_2PO_4x2H_2O$,20 mg/L) and the main algal species identified by means of optical microscopy (Leica DM2500 optical microscope).

2.4. Accelerated weathering test

The previously prepared algae cultures were employed to perform an accelerated weathering test on limestones by immersing stone slabs (1.5 x 1.5 x 0.5 cm) inside a culture tank at room temperature for 28 days with permanent lighting (tungsten-halogen filament lamp whose emission of UV radiation is about 2% of total emission [40], 100W). At the end of this period the stone slabs were allowed to dry for 5 days at room temperature. Additionally, accelerated weathering tests on treated slabs were performed to establish the capability of the nanocomposites to inhibit biopatina growth on limestones by depositing doses up to 200 µL of a water suspension of the nanocomposite on the stone slab surface, and allowing the spot to dry at room temperature before immersing the slide in the tank. The concentration of the nanoparticle suspension was adjusted to obtain 0.03 mg/mL referred to silver. The surfaces of the samples were analyzed before and after the accelerated weathering test by means of a Zarbeco handheld digital microscope and a Leica DM4500M optical microscope to determine the appearance of biofilms, and a colorimeter X-Rite SP60 to evaluate chromatic changes induced by the nanocomposites and/or the generation of biopatina. Untreated stones, subjected to the accelerated weathering test, when required, were used as control for the chromatic changes determinations.

Chromatic changes (ΔE^*) were calculated according to the parameters defined by the CIELAB color-system according to Eq. (1).

$$\Delta E^* = \sqrt{\Delta L^{*2} + \Delta a^{*2} + \Delta b^{*2}} \qquad \text{Eq. (1)}$$

Where ΔL^*, Δa^* and Δb^* characterize variations of the color values as referred to the control in the black-white (brightness), red-green and yellow-blue axes, respectively.

3. Results and discussion

3.1. Treatments

Silver nanoparticles, TiO_2 nanoparticles and silver/TiO_2-nanocomposites have been selected to evaluate their effectiveness in preventing biopatina growth on limestone. Silver/TiO_2-nanocomposites were obtained by reducing silver nitrate with a strong reducing agent, sodium borohydride, in an aqueous medium containing TiO_2 nanoparticles. Different nanocomposites were prepared by varying the molar ratio Ag:TiO_2 (Table 1) and, additionally, a set of nanocomposites was prepared by introducing a second additive, citrate, during the reduction process. We have chosen citrate because it is a stabilizing agent widely employed in the synthesis of silver nanoparticles, in order to diminish the hydrodynamic diameter of nanocomposites, as we will discuss later on. Regarding TiO_2, our source was P-25 from Degussa. We have chosen P-25 because it is a standard material widely employed in photocatalytic applications [41], including the photodegradation of organic matter [42]. P-25 contains anatase and rutile phases in a 3:1 ratio, with average sizes of 85 and 25 nm, respectively, as determined by transmission electron microscopy [43].

Table 1. Molar Ag:TiO_2 ratio, hydrodynamic diameter (HD) and zeta potential (ζ) of the different types of nanocomposites compared to TiO_2 and Ag@cit nanoparticles.

Treatment	Ag:TiO_2	HD (nm)	ζ (mV)
TiO_2	-	184±49	-17±2
Ag@cit	-	36±8	-63±3
Ag@cit/TiO_2	0.04	72±18	-24.8±0.3
2xAg@cit/TiO_2	0.08	52±11	-27±1
Ag/TiO_2	0.04	234±32	-16±1
2xAg/TiO_2	0.08	170±26	-17±1
4xAg/TiO_2	0.16	94±33	-17±3

In summary, we have developed two types of treatments based on silver/TiO_2-nanocomposites, one based on silver nanoparticles stabilized by citrate and one based on naked silver nanoparticles. In addition to nanocomposites we have also assayed silver and TiO_2 nanoparticles to unpick the effect in isolation versus in combination.

As can be seen in Table 1, the least favorable HDs are obtained for TiO_2 nanoparticles and naked-silver nanocomposites. Their high HD and low zeta potential are indicative of low colloidal stability and aggregation [44]. Far more favorable HDs are achieved by citrate-stabilized silver nanocomposites owing to the stabilizing effect of trisodium citrate. In fact, Ag@cit nanoparticles show the lowest HD and extreme zeta potential (-63 mV). Moreover, Ag@cit nanoparticles have a narrow surface plasmon peaking at 400 nm (Fig. S.1), which indicates that they are small and have a narrow size distribution. Nanocomposites obtained from citrate-stabilized silver nanoparticles exhibit higher stability in aqueous medium than those obtained from naked silver nanoparticles. As in the case of Ag@cit nanoparticles, their TiO_2-derived nanocomposites show a silver plasmon peaking at 400 nm, whereas naked-silver nanocomposites plasmon peaking appears at higher wavelength, 440 nm, indicating that the size of the latter is larger (Fig. S.1). These results are in good agreement with the values of HD (Table 1). It is worth noting that both for Ag@cit and naked-silver nanocomposites, decreasing the molar ratio Ag:TiO_2 (i.e. the amount of silver in the formulation) leads to destabilization of the resulting nanocomposites as evidenced by the increase in HD and zeta potentials closer to zero [30].

The TEM analysis of both composites indicates that the samples are formed by agglomerated TiO_2 and Ag particles. An example of each type of nanocomposite is shown in Figures 2.a and 3a. Rounded silver nanocrystals (darker contrast) are deposited on top of the TiO_2 nanoplatelets; therefore, it was difficult to measure the Ag interplanar spacing. However in the Ag/TiO_2 composite it was possible to found a small nanocrystal of silver (marked square) with cubic structure (space group 225=Fm-3m; cell parameter a=4.09 Å) as can be seen in the HRTEM image presented in Fig. 2.b; such Ag crystal is oriented along the [1 0 1] zone axis as indicate the inset FFT. In the case of Ag@cit/TiO_2 composite only (2 0 0) silver planes were measured, marked in the micrograph presented in Fig. 3.b. TiO_2 nanocrystals present faceted shape and correspond with the lighter contrast in the TEM images. In Figures 2.d, 3.c and 3.d, three HRTEM micrographs of some of these nanoplatelets are presented. Which are oriented along the [1 1 1] zone axis for Ag/TiO_2 and along [1 0 0] and [1 0 1] for Ag@cit/TiO_2, and belong to the tetragonal structure of Anatase (space group 141 = I41 / amd; parameters of cell a = 3.78 and c = 9.51Å), the corresponding FFT are inserted.

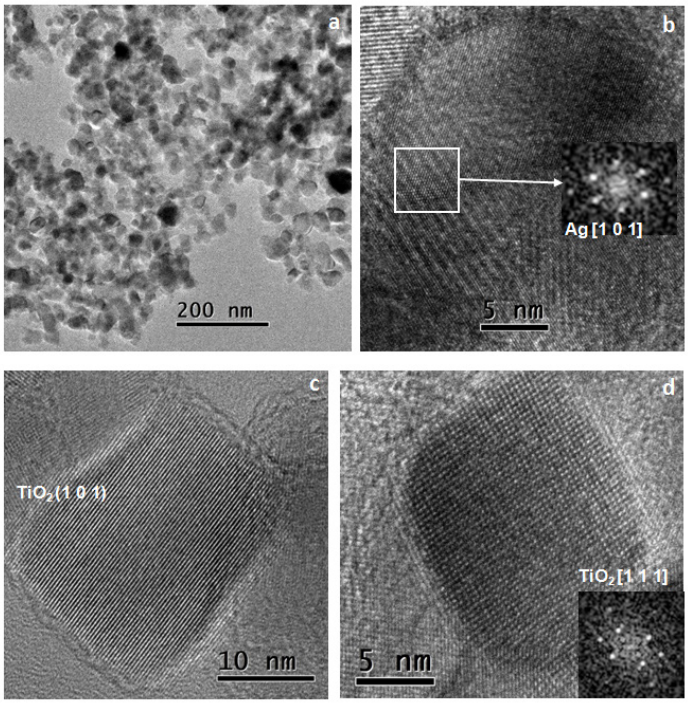

258

259 **Fig. 2.** (a) TEM image of the Ag/TiO_2 composite; (b) HRTEM image showing a silver crystallite (square
260 marked) oriented along [1 0 1], the corresponding FFT is inset; (c) HRTEM micrograph of TiO_2 nanocrystal
261 with the (1 0 1) planes marked and (d) TiO_2 crystallite oriented along [1 1 1] zone axes and FFT inset.

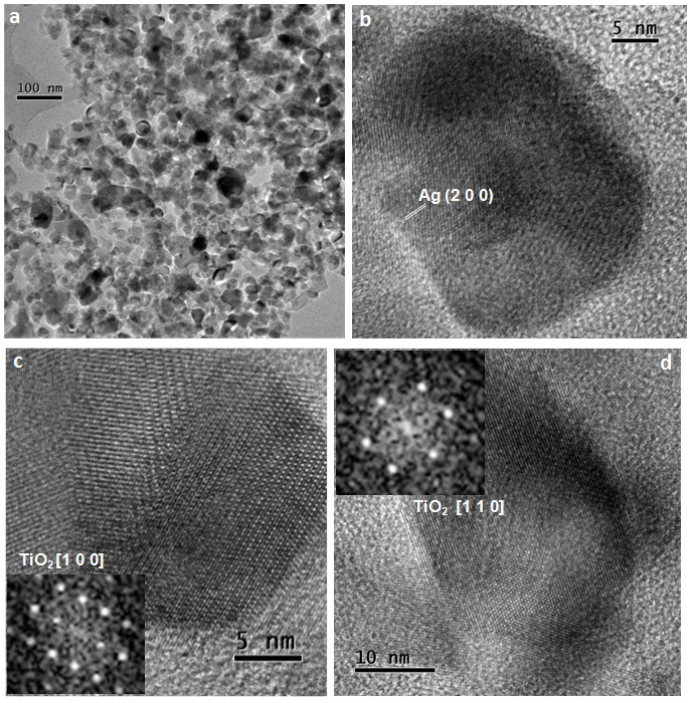

262

263 **Fig. 3.** (a) TEM image of the Ag@cit/TiO_2 composite; (b) HRTEM micrograph showing a silver nanocrystal
264 and (c and d) HRTEM images of TiO_2 nanocrystals oriented along [1 0 0] and [1 1 0] zone axes respectively,
265 the corresponding FFT are inset.

The chemical microanalysis was carried out using an EDS spectroscopic technique in STEM mode (HAAD detector) and the most representative results are shown in Figures 4 and 5. At this point it is important to note that the image contrast obtained in TEM and STEM is inverse, In TEM images, the darker contrast corresponds to heavier elements while in STEM images corresponds to lighter elements, due to the different detectors used to get the images.

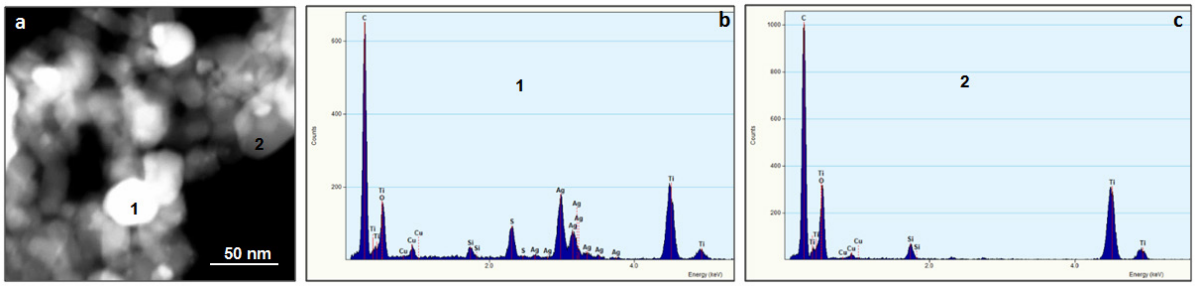

Fig. 4. (a) STEM image of the Ag/TiO_2 composite and (b and c) EDX spectra corresponding to points one and two respectively, marked in the STEM image.

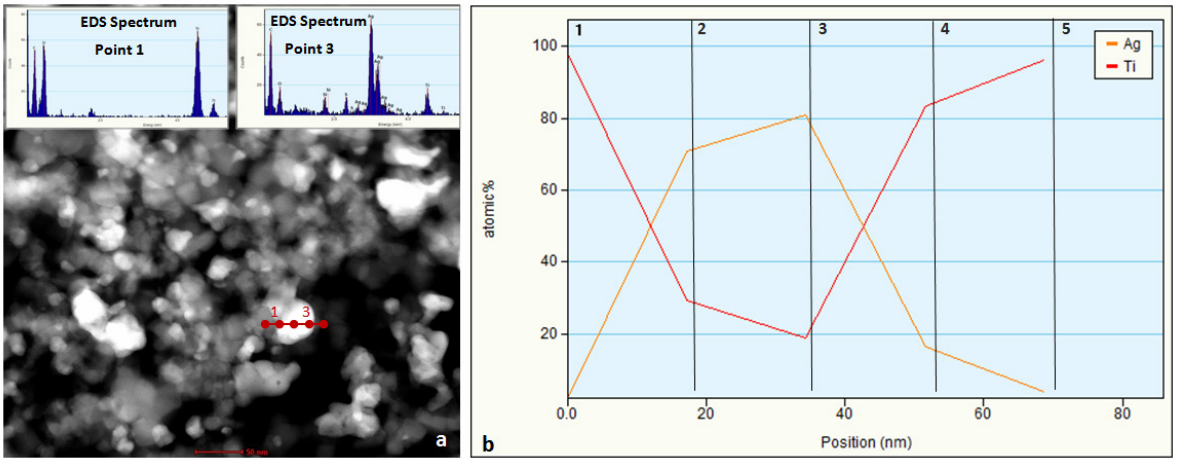

Fig. 5. (a) STEM image of the Ag@cit/TiO_2 composite (the red line corresponds to the EDX profile; five point analysis) and EDX spectra of point 1 (top inset) and point 3 (bottom inset). (b) Ti/Ag atomic percentage ratio along the profile

An EDS analysis of the Ag/TiO_2 composite was done in two different positions, one in a bright contrast particle and another in a dark contrast particle, marked in the STEM image presented in Fig. 4.a (1 and 2 respectively). The obtained spectra for both positions are depicted in Fig. 4.b and 4.c, the brighter position (1) clearly corresponds to a silver nanocrystal on the top of TiO_2 particles, and

282 position two belongs to a TiO_2 nanoplatelet. The C-K and Cu-K picks are coming from the grid. A
283 composition profile was made for the Ag@cit/TiO_2 composite along the red line marked in the STEM
284 micrograph (Fig. 5.a). Figure 5.b shows the Ti/Ag atomic percentage along such profile (five points
285 were analyzed). The obtained EDS spectra recorded in point one and three are inset in the top and
286 bottom of the Fig. 5.a respectively. In the same way that the previous composite, the darker contras
287 (point 1) belongs to a TiO_2 nanoplatelet and the lighter contrast (point 3) corresponds to a silver
288 crystal, which is located on the top of TiO_2 particles. In addition to Ti, O and Ag elements, carbon was
289 also found in the analyzed profile; C element must come from the citrate molecules as the C from the
290 grid is discarded since the analyzed area was supported on a hole. Si and S elements must be
291 impurities in both composites.

292 *3.2. Biopatina characterization and use in accelerated weathering*

293 On site diagnosis of the thirty churches studied in Seville show that biopatina and vegetation
294 appear in 90% of these buildings (Fig.6), that means that 27 of the 30 churches studied need a
295 preventive conservation treatment against biocolonization. The frequency of the biocrust is low and
296 medium, and the frequency of vegetation is mainly low and medium, although it reaches high levels if
297 preventive conservation of roofs is not carried out. Moreover, the frequency of these weathering forms
298 change on the walls of a same building, as the distribution of these pathologies depends on the
299 orientation; they appear commonly on Northern and Southern walls, and on the dampness due to
300 drainpipes, water sprouts or capillarity.

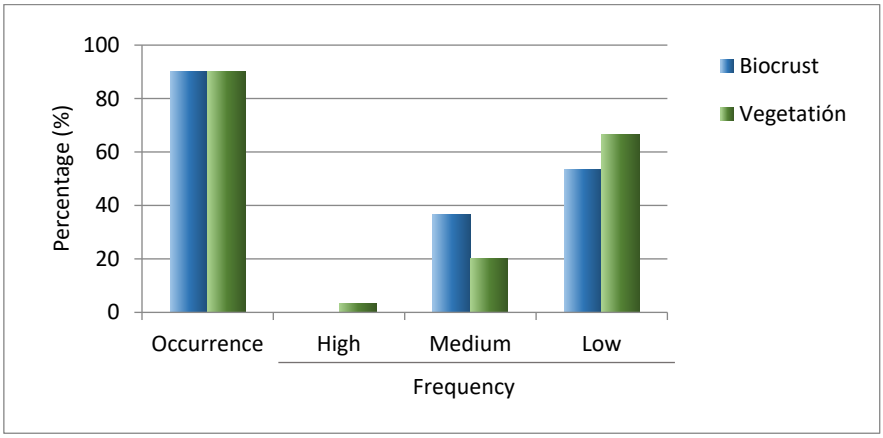

301

302 **Fig. 6.** Vulnerability to biocrust (blue bars) and vegetation (green bars) in thirty churches studied in Seville.

In order to achieve a representative green biopatina culture for the biocrust that develops in the climatic conditions of Seville, samples taken from the façades of different churches in Seville have been collected, characterized and grown to obtain a culture. These façades were built with limestones, sandstones and calcarenites similar to slabs from Utrera (Spain)[38]. The samples were collected in different conditions and times (autumn and spring according to the rain periods in Seville).

The SEM study of the samples showed that these biopatinas are spread on high porosity substrates generating biological deposits with thicknesses between 10-400μm (Fig. S.2.a). Furthermore, highly porous stones favor the penetration of microorganisms through intergranular areas causing fissures and powdering (Fig. S.2.b), two of the most important physical damages associated to this kind of alteration agent. The results of the EDX analysis show only silicon (Si) and Calcium (Ca) in the composition of the samples (Fig. S.2.c), corroborating that the damages of these biopatinas and biocrusts are only physical and aesthetic because no sub-products of alteration have been identified..

Green biocrust samples were grown, thoroughly mixed and cultured. The rich mixture contained viable micro-organisms that had proven to be especially adapted to grow on limestone, covering a broad range of environmental and surface conditions, and are therefore deemed to be suitable for a quick colonization of fresh limestone slabs. This formed the basis for our accelerated weathering test.

Five types of green algae (Chlorophyta) were identified in the culture, corresponding to species of the genera Chlorella, Botryococcus, Cyclotella, Monoraphidium and phytoflagellate and two blue-green algae (Cyanobacteria) corresponding to the species of the genera Gloeocapsa and Nostoc.

3.3. Aesthetical impact of the treatments to inhibit biopatina

The chromatic changes in stone slabs were measured after the application of nanocomposites both before (ante weathering, aw) and after (post weathering, pw) weathering tests. Measures taken ante weathering test have the purpose of evaluating the initial aesthetic impact of the different treatments on the stone, while measures taken post weathering test show the effectiveness of treatments as inhibitors of the formation of biopatina. Table 2 shows the chromatic coordinate

330 increments ΔL*, Δa*and Δb* obtained for the stone slabs ante and post-weathering tests, as well as the
331 corresponding ΔE*, calculated according to Eq.1, and the total increments.

332 **Table 2.** Increases of color caused by the application of nanocomposites and the generation of
333 biopatina

	ante-Weathering test [aw]				*post-Weathering test [pw]*				*Final increments*			
Product	*ΔL**	*Δa**	*Δb**	*ΔE**	*ΔL**	*Δa**	*Δb**	*ΔE**	*ΔL**	*Δa**	*Δb**	*ΔE**
TiO₂	*0.31*	*-0.10*	*-0.77*	*0.84*	*-8.09*	*6.7*	*14.52*	*17.92*	*-7.78*	*6.60*	*13.75*	*17.12*
Ag@cit	*-5.92*	*0.72*	*3.05*	*6.69*	*-7.25*	*6.89*	*15.21*	*18.20*	*-13.17*	*7.61*	*18.26*	*23.76*
Ag@cit/TiO₂	*-8.40*	*2.37*	*5.13*	*10.12*	*-3.64*	*2.35*	*1.75*	*4.67*	*-12.04*	*4.72*	*6.88*	*14.65*
2xAg@cit/TiO₂	*-8.07*	*1.50*	*2.70*	*8.63*	*-1.32*	*2.2*	*4.42*	*5.11*	*-9.39*	*3.70*	*7.12*	*12.34*
Ag/TiO₂	*-19.12*	*8.40*	*12.30*	*24.24*	*-5.51*	*-3.78*	*-1.47*	*6.84*	*-24.63*	*4.62*	*10.38*	*27.30*
2xAg/TiO₂	*-9.38*	*4.61*	*9.15*	*13.89*	*-8.26*	*0.85*	*10.01*	*13.01*	*-17.64*	*5.46*	*19.16*	*26.61*
4xAg/TiO₂	*-4.97*	*0.99*	*0.88*	*5.14*	*-14.47*	*7.84*	*17.93*	*24.34*	*-19.44*	*8.83*	*18.81*	*28.46*
Untreated sample	*-*	*-*	*-*	*-*	*-18.66*	*5.47*	*17.88*	*26.42*	*-18.66*	*5.47*	*17.88*	*26.42*

334

335 The visual impact of treatment is shown in Figure 7, in which stone slabs are shown after the
336 deposition of the different treatments. Ag/TiO_2 and $2xAg/TiO_2$ nanocomposites exhibit a noticeable
337 change in color when compared to control. This is in keeping with data quantified using ΔE*[aw] tool.

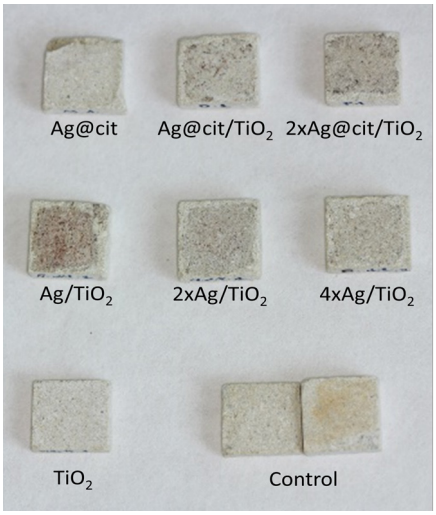

338

339 **Fig. 7.** Digital photographs of limestone slabs after the application of treatments (200 μL of an aqueous
340 suspension of nanocomposites). All of the silver-bearing treatments have the same silver dose.

341 Remarkably, the chromatic changes (a* and b*) produced by the application of the treatments
342 (Fig. 8) remain within the range of variability of the control untreated limestone from Utrera, except
343 for Ag/TiO_2 and $2xAg/TiO_2$. These nanocomposites are significantly shifted to higher values (i.e. red
344 and yellow). Other treatments remain close to the chromatic values of the untreated limestone.

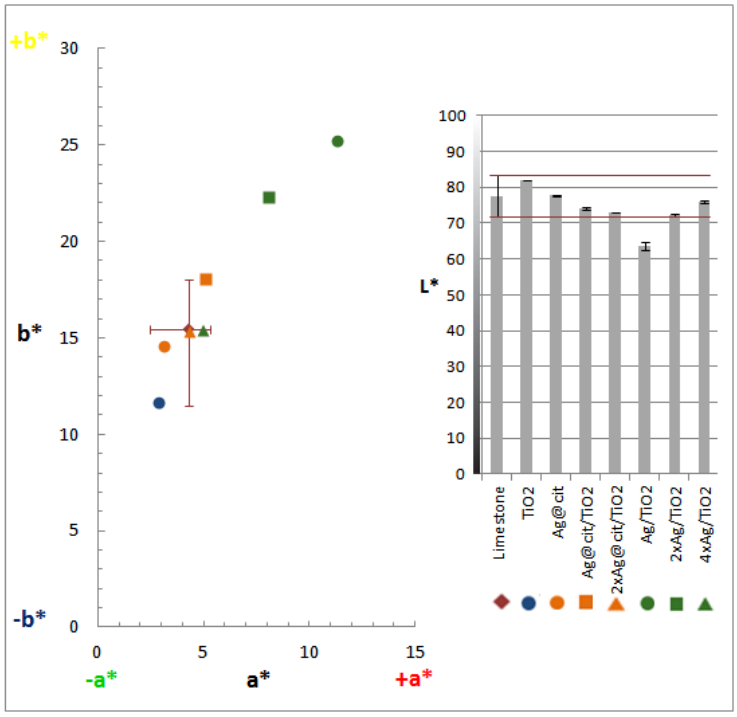

345

346 **Fig. 8.** Chromatic changes a*/b* and brightness L* (inset) of the limestone slabs following treatment (ante-
347 weathering test). Red lines highlight the variability of the untreated stone samples.

348 The effect of initial treatment on the ΔL* variable is generally negative causing darkening,
349 excepted for Ag@cit and TiO_2. For other samples, the darkening remains within the variability range
350 of the untreated stone (Figure 8, inset).

351 The high color change originated by Ag/TiO_2 and $2xAg/TiO_2$ nanocomposites, when
352 compared to $4xAg/TiO_2$, can be explained based on their colloidal stability. $4xAg/TiO_2$ nanocomposite
353 has a smaller hydrodynamic diameter and similar zeta potential than its analogues Ag/TiO_2 and
354 $2xAg/TiO_2$, and is therefore expected to be more stable. Moreover, the concentration of the aqueous
355 suspension of all nanocomposites was adjusted to obtain 0.03 mg/mL (referred to silver) in the assays.
356 The TiO_2 amount was 0.53 mg/mL in the sample without silver, in Ag/TiO_2 and in $Ag@cit/TiO_2$,
357 whereas in suspensions with higher relative silver amounts (doubled and quadrupled) than that of their
358 analogues, the TiO_2 amount is therefore lowered in the same proportion. As a consequence, both
359 Ag/TiO_2 and $2xAg/TiO_2$ aggregate and excess nanocomposite precipitates, they saturate the pores on
360 the stone surface and bring about a change in color (Fig. 9).

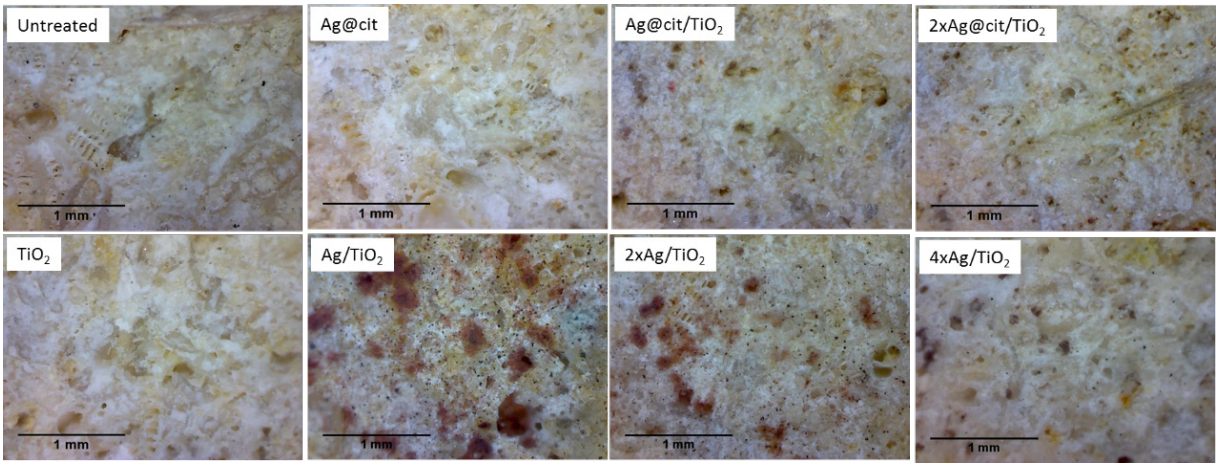

Fig. 9. Magnified (140x) stone surfaces after treatment, analyzed by Zarbeco handheld digital microscope

In the case of citrate-capped silver/TiO_2 nanocomposites the situation is similar; however, as these nanocomposites are much smaller and more stable than the related nanocomposites obtained from naked-silver nanoparticles, the effect is not so remarkable. The general trend of nanocomposites to aggregate after deposition is also observed by SEM (Fig. S.3).

3.4. Effectiveness of the treatments in accelerated weathering test

As mentioned above, the suitability of the nanocomposites to inhibit the generation of biopatina was assayed by means of spectrophotometric color measurements, a method that is emerging as an improved alternative to previous methods such as chlorophyll α determination or fluorescein diacetate hydrolysis [45–48]. Among the advantages of the spectrophotometric color measurement method, it should be noted that it is a non-destructive technique that can be performed on-site, not requiring expensive and time-consuming sample preparation [46–48].

Three ΔE* values have been calculated, the first one before the weathering test ΔE*[aw], the second one after the weathering test ΔE*[pw] and the third one ΔE*[t]. ΔE*[aw] characterizes the initial aesthetical impact of treatment, as it measures the chromatic change from untreated stone slabs to freshly treated slabs, ΔE*[pw] from freshly treated slabs to weathered slabs, and ΔE*[t] describes the overall change from untreated slabs to treated and weathered ones. Fig. 10 summarizes the chromatic changes for the treatments studied. Although there is no standardized rule for the interpretation of color changes in Cultural Heritage materials as a result of the application of biocide products, three ranges of chromatic changes have been proposed for dyes in Cultural Heritage porous

materials: ΔE*<5, chromatic changes cannot be detected by the human eye; 5<ΔE*<10, chromatic changes can be detected by the human eye but still acceptable; and ΔE*>10, chromatic changes are clearly visible [49]. This global color variation, ΔE*<10, has also been established as threshold by other authors [50]. In our case, the initial aesthetic impact of the different treatments on the stone, i.e. *ante*-weathering test, have a global color variation ΔE*[aw]<10 except for Ag/TiO_2 and 2xAg/TiO_2 nanocomposites TiO_2 nanoparticles and the 4xAg/TiO_2 nanocomposite achieve ΔE*[aw]<5.

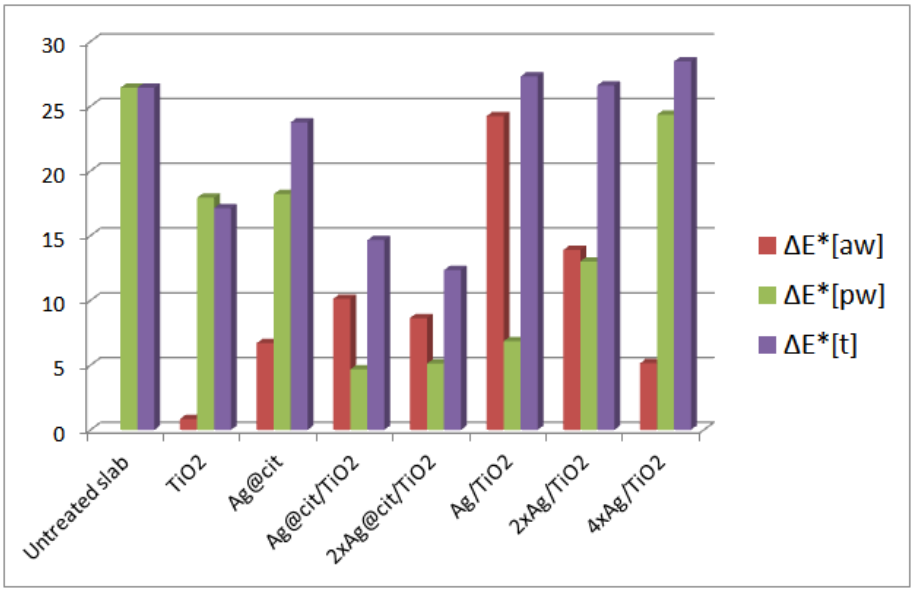

Fig. 10. ΔE*[aw], ΔE*[pw] and ΔE*[t] for the different treatments.

As can be seen in Figure 10, both TiO_2 and Ag@cit nanoparticles inhibit the biopatina growth. Nevertheless, the extent of this inhibition is modest, and ΔE*[pw] is reduced by only 25-30%, as referred to the untreated sample. On the other hand, the combination of these active ingredients into a nanocomposite, Ag@cit/TiO_2 nanocomposites, greatly increases the effectiveness of treatment when compared to nanoparticles themselves so that ΔE* is reduced by over 80%. Due to this synergy, increasing the Ag:TiO_2 ratio does not slow down biopatina growth, as can be seen in Figure 10. This synergy could be due to a lowering by silver of the band gap in TiO_2 [27].

On the other hand, the overall chromatic changes, ΔE*[t], were smaller in the treated slabs when compared to the untreated ones, except for the naked silver/TiO_2 nanocomposites. Remarkably, above 80% reduction in biopatina formation was achieved by Ag@cit/TiO_2 and 2xAg@cit/TiO_2 nanocomposites, with ΔE[t]* values close to 10.

4. Conclusions

A variety of treatments that we designed to prevent biopatina formation on limestone were investigated. The initial impact was assessed, and then the stone slabs, which stem from a quarry in Utrera, were subjected to accelerated weathering. The accelerated weathering test used real-world algae grown on historical monuments affected by biodeterioration. Whereas both silver nanoparticles and titanium dioxide P25 nanoparticles achieved some degree of inhibition on their own, it was the combination of both in a small-size, stable, citrate promoted nanocomposite that achieved a very significant reduction. These nanocomposites minimize the aesthetical impact on the surfaces on which they were applied. They can be prepared in an aqueous medium, avoiding the need for organic solvents. They could be applied both by spray or by brush, or be mixed with other formulations such as mortars to confer them biocide properties as preventive conservation measures.

Acknowledgements

This study has been partially supported by the projects: Art-Risk, RETOS project of Ministerio de Economía y Competitividad and Fondo Europeo de Desarrollo Regional (FEDER), (code: BIA2015-64878-R (MINECO/FEDER, UE)), CTQ2013-48396-P of Fondo Europeo de Desarrollo Regional (FEDER-Unión Europea) and Ministerio Economía y Competitividad and the research teams P10-FQM-6615, TEP-199 and FQM-319 from Junta Andalucía. J. Becerra is grateful to the Ministerio de Educación, Cultura y Deporte for his pre-doctoral fellowship.

Bibliography

[1] *M.F. Macedo, A.Z. Miller, A. Dionisio, C. Saiz-Jimenez, Biodiversity of cyanobacteria and green algae on monuments in the Mediterranean Basin: An overview, Microbiology. 155 (2009) 3476–3490. doi:10.1099/mic.0.032508-0.*

[2] *C. Gaylarde, M. Ribas Silva, T. Warscheid, Microbial impact on building materials: an overview, Mater. Struct. 36 (2003) 342–352. doi:10.1007/BF02480875.*

[3] *Y. Nuhoglu, E. Oguz, H. Uslu, A. Ozbek, B. Ipekoglu, I. Ocak, I. Hasenekoglu, The accelerating effects of*

the microorganisms on biodeterioration of stone monuments under air pollution and continental-cold climatic conditions in Erzurum, Turkey, Sci. Total Environ. 364 (2006) 272–283. doi:10.1016/j.scitotenv.2005.06.034.

[4] K. Sterflinger, G. Piñar, Microbial deterioration of cultural heritage and works of art - Tilting at windmills?, Appl. Microbiol. Biotechnol. 97 (2013) 9637–9646. doi:10.1007/s00253-013-5283-1.

[5] C.A. Crispim, C.C. Gaylarde, Cyanobacteria and biodeterioration of cultural heritage: A review, Microb. Ecol. 49 (2005) 1–9. doi:10.1007/s00248-003-1052-5.

[6] J.P. Calvo, M. Regueiro, Carbonate rocks in the Mediterranean region - from classical to innovative uses of building stone, Geol. Soc. London, Spec. Publ. 331 (2010) 27–35. doi:10.1144/sp331.3.

[7] M.P. Nugari, O. Salvadori, Biocides and Treatment of Stone: Limitations and Future Prospects, in: R.J. Koestler, V.H. Koestler, A.E. Charola, F. Nieto-Fernandez (Eds.), Art, Biol. Conserv. Biodeterior. Work. Art, The Metropolitan Museum of Art, New York, 2003: pp. 518–535.

[8] F. Bastian, V. Jurado, A. Nováková, C. Alabouvette, C. Saiz-Jimenez, The microbiology of Lascaux Cave, Microbiology. 156 (2010) 644–652. doi:10.1099/mic.0.036160-0.

[9] F. Bellissima, M. Bonini, R. Giorgi, P. Baglioni, G. Barresi, G. Mastromei, B. Perito, Antibacterial activity of silver nanoparticles grafted on stone surface, Environ. Sci. Pollut. Res. 21 (2014) 13278–13286. doi:10.1007/s11356-013-2215-7.

[10] A.M.M. Essa, M.K. Khallaf, Biological nanosilver particles for the protection of archaeological stones against microbial colonization, Int. Biodeterior. Biodegrad. 94 (2014) 31–37. doi:10.1016/j.ibiod.2014.06.015.

[11] B. Gutarowska, J. Skora, K. Zduniak, D. Rembisz, Analysis of the sensitivity of microorganisms contaminating museums and archives to silver nanoparticles, Int. Biodeterior. Biodegrad. 68 (2012) 7–17. doi:10.1016/j.ibiod.2011.12.002.

[12] J.S. Kim, E. Kuk, K.N. Yu, J.H. Kim, S.J. Park, H.J. Lee, S.H. Kim, Y.K. Park, Y.H. Park, C.Y. Hwang, Y.K. Kim, Y.S. Lee, D.H. Jeong, M.H. Cho, Antimicrobial effects of silver nanoparticles, Nanomedicine Nanotechnology, Biol. Med. 3 (2007) 95–101. doi:10.1016/j.nano.2006.12.001.

[13] E. Cavaliere, S. De Cesari, G. Landini, E. Riccobono, L. Pallecchi, G.M. Rossolini, L. Gavioli, Highly

bactericidal Ag nanoparticle films obtained by cluster beam deposition, Nanomedicine Nanotechnology, Biol. Med. 11 (2015) 1417–1423. doi:10.1016/j.nano.2015.02.023.

[14] C.-N. Lok, C.-M. Ho, R. Chen, Q.-Y. He, W.-Y. Yu, H. Sun, P.K.-H. Tam, J.-F. Chiu, C.-M. Che, Silver nanoparticles: partial oxidation and antibacterial activities, JBIC J. Biol. Inorg. Chem. 12 (2007) 527–534. doi:10.1007/s00775-007-0208-z.

[15] I. Sondi, B. Salopek-Sondi, Silver nanoparticles as antimicrobial agent: A case study on E. coli as a model for Gram-negative bacteria, J. Colloid Interface Sci. 275 (2004) 177–182. doi:10.1016/j.jcis.2004.02.012.

[16] S. Pal, Y.K. Tak, J.M. Song, Does the Antibacterial Activity of Silver Nanoparticles Depend on the Shape of the Nanoparticle? A Study of the Gram-Negative Bacterium Escherichia coli, Appl. Environ. Microbiol. 73 (2007) 1712–1720. doi:10.1128/AEM.02218-06.

[17] P. Van Dong, C. Ha, L. Binh, J. Kasbohm, Chemical synthesis and antibacterial activity of novel-shaped silver nanoparticles, Int. Nano Lett. 2 (2012) 9. doi:10.1186/2228-5326-2-9.

[18] M. Rai, A. Yadav, A. Gade, Silver nanoparticles as a new generation of antimicrobials, Biotechnol. Adv. 27 (2009) 76–83. doi:10.1016/j.biotechadv.2008.09.002.

[19] E. Quagliarini, F. Bondioli, G.B. Goffredo, A. Licciulli, P. Munafò, Smart surfaces for architectural heritage: Preliminary results about the application of TiO2-based coatings on travertine, J. Cult. Herit. 13 (2012) 204–209. doi:10.1016/j.culher.2011.10.002.

[20] E. Quagliarini, F. Bondioli, G.B. Goffredo, C. Cordoni, P. Munafò, Self-cleaning and de-polluting stone surfaces: TiO2 nanoparticles for limestone, Constr. Build. Mater. 37 (2012) 51–57. doi:10.1016/j.conbuildmat.2012.07.006.

[21] P. Munafò, G.B. Goffredo, E. Quagliarini, TiO2-based nanocoatings for preserving architectural stone surfaces: An overview, Constr. Build. Mater. 84 (2015) 201–218. doi:10.1016/j.conbuildmat.2015.02.083.

[22] F. Pacheco-Torgal, S. Jalali, Nanotechnology: Advantages and drawbacks in the field of construction and building materials, Constr. Build. Mater. 25 (2011) 582–590. doi:10.1016/j.conbuildmat.2010.07.009.

481 [23] L. Graziani, E. Quagliarini, F. Bondioli, M. D'Orazio, Durability of self-cleaning TiO2 coatings on fired
482 clay brick façades: Effects of UV exposure and wet & dry cycles, Build. Environ. 71 (2014) 193–203.
483 doi:10.1016/j.buildenv.2013.10.005.

484 [24] P. Munafò, E. Quagliarini, G.B. Goffredo, F. Bondioli, A. Licciulli, Durability of nano-engineered TiO2
485 self-cleaning treatments on limestone, Constr. Build. Mater. 65 (2014) 218–231.
486 doi:10.1016/j.conbuildmat.2014.04.112.

487 [25] M.F. La Russa, S.A. Ruffolo, N. Rovella, C.M. Belfiore, A.M. Palermo, M.T. Guzzi, G.M. Crisci,
488 Multifunctional TiO2 coatings for Cultural Heritage, Prog. Org. Coatings. 74 (2012) 186–191.
489 doi:10.1016/j.porgcoat.2011.12.008.

490 [26] H.A. Foster, I.B. Ditta, S. Varghese, A. Steele, Photocatalytic disinfection using titanium dioxide:
491 Spectrum and mechanism of antimicrobial activity, Appl. Microbiol. Biotechnol. 90 (2011) 1847–1868.
492 doi:10.1007/s00253-011-3213-7.

493 [27] M.F. La Russa, A. Macchia, S.A. Ruffolo, F. De Leo, M. Barberio, P. Barone, G.M. Crisci, C. Urz??,
494 Testing the antibacterial activity of doped TiO2 for preventing biodeterioration of cultural heritage
495 building materials, Int. Biodeterior. Biodegrad. 96 (2014) 87–96. doi:10.1016/j.ibiod.2014.10.002.

496 [28] Y. Zhao, B. Yang, J. Xu, Z. Fu, M. Wu, F. Li, Facile synthesis of Ag nanoparticles supported on TiO 2
497 inverse opal with enhanced visible-light photocatalytic activity, Thin Solid Films. 520 (2012) 3515–
498 3522. doi:10.1016/j.tsf.2011.12.076.

499 [29] I. Yaşa, N. Lkhagvajav, M. Koizhaiganova, E. Çelik, Ö. Sari, Assessment of antimicrobial activity of
500 nanosized Ag doped TiO2 colloids, World J. Microbiol. Biotechnol. 28 (2012) 2531–2539.
501 doi:10.1007/s11274-012-1061-y.

502 [30] M. Lungu, Ş. Gavriliu, E. Enescu, I. Ion, A. Brătulescu, G. Mihăescu, L. Măruţescu, M.C. Chifiriuc,
503 Silver-titanium dioxide nanocomposites as effective antimicrobial and antibiofilm agents, J.
504 Nanoparticle Res. 16 (2014). doi:10.1007/s11051-013-2203-3.

505 [31] Y. Lin, W. Qiqiang, Z. Xiaoming, W. Zhouping, X. Wenshui, D. Yuming, Synthesis of Ag/TiO 2
506 Core/Shell Nanoparticles with Antibacterial Properties, Bull. Korean Chem. Soc. 32 (2011) 2607–2610.
507 doi:10.5012/bkcs.2011.32.8.2607.

508 [32] D. Nithyadevi, P. Suresh Kumar, D. Mangalaraj, N. Ponpandian, C. Viswanathan, P. Meena, Improved

microbial growth inhibition activity of bio-surfactant induced Ag-TiO2 core shell nanoparticles, Appl. Surf. Sci. 327 (2015) 504–516. doi:10.1016/j.apsusc.2014.11.169.

[33] X.H. Yang, H.T. Fu, X.C. Wang, J.L. Yang, X.C. Jiang, A.B. Yu, Synthesis of silver-titanium dioxide nanocomposites for antimicrobial applications, J. Nanoparticle Res. 16 (2014). doi:10.1007/s11051-014-2526-8.

[34] M.A. Guerrero Montes, Diagnóstico del estado de alteración de la piedra del palacio consistorial de Sevilla. Causas y mecanismos., University of Seville, 1990.

[35] M.Á. Bello López, Caracterización y estado de alteración química de los materiales empleados en la construción de la Catedral de Sevilla, Univerisdad de Sevilla, 1988.

[36] P. Ortiz, M.A. Guerrero, M.A. Vázquez, R. Ortiz, J.M. Martín, M.C. Peña, Accelerated weathering test as environmental behaviour trials on calcareous stone, in: Proceeding 11th Int. Congr. Deterior. Conserv. Stone., 2008: pp. 223–231.

[37] C.Y. Flores, C. Diaz, A. Rubert, G.A. Benítez, M.S. Moreno, M.A. Fernández Lorenzo de Mele, R.C. Salvarezza, P.L. Schilardi, C. Vericat, Spontaneous adsorption of silver nanoparticles on Ti/TiO2 surfaces. Antibacterial effect on Pseudomonas aeruginosa, J. Colloid Interface Sci. 350 (2010) 402–408. doi:10.1016/j.jcis.2010.06.052.

[38] F. Colao, R. Fantoni, P. Ortiz, M.A. Vazquez, J.M. Martin, R. Ortiz, N. Idris, Quarry identification of historical building materials by means of laser induced breakdown spectroscopy, X-ray fluorescence and chemometric analysis, in: Spectrochim. Acta - Part B At. Spectrosc., 2010: pp. 688–694. doi:10.1016/j.sab.2010.05.005.

[39] R. Ortiz, P. Ortiz, Vulnerability Index: a new approach for preventive conservation of monuments., Int. J. Archit. Herit. (2016). doi:10.1080/15583058.2016.1186758.

[40] T.T. Schaeffer, Effects of Light on Materials in Collections : Data on Photoflash and Related Sources by Effects, 2001. http://ccl.worldcat.org/oclc/46785588.

[41] A. Ibhadon, P. Fitzpatrick, Heterogeneous Photocatalysis: Recent Advances and Applications, Catalysts. 3 (2013) 189–218. doi:10.3390/catal3010189.

[42] A. Mills, S. Le Hunte, An overview of semiconductor photocatalysis, J. Photochem. Photobiol. A Chem.

536 108 (1997) 1–35. doi:10.1016/S1010-6030(97)00118-4.

537 [43] T. Ohno, K. Sarukawa, K. Tokieda, M. Matsumura, Morphology of a TiO2 Photocatalyst (Degussa, P-
538 25) Consisting of Anatase and Rutile Crystalline Phases, J. Catal. 203 (2001) 82–86.
539 doi:10.1006/jcat.2001.3316.

540 [44] K. Suttiponparnit, J. Jiang, M. Sahu, S. Suvachittanont, T. Charinpanitkul, P. Biswas, Role of Surface
541 Area, Primary Particle Size, and Crystal Phase on Titanium Dioxide Nanoparticle Dispersion
542 Properties, Nanoscale Res. Lett. 6 (2011) 1–8. doi:10.1007/s11671-010-9772-1.

543 [45] B. Prieto, B. Silva, O. Lantes, Biofilm quantification on stone surfaces: Comparison of various methods,
544 Sci. Total Environ. 333 (2004) 1–7. doi:10.1016/j.scitotenv.2004.05.003.

545 [46] W. De Muynck, A.M. Ramirez, N. De Belie, W. Verstraete, Evaluation of strategies to prevent algal
546 fouling on white architectural and cellular concrete, Int. Biodeterior. Biodegrad. 63 (2009) 679–689.
547 doi:10.1016/j.ibiod.2009.04.007.

548 [47] P. Sanmartín, D. Vázquez-Nion, B. Silva, B. Prieto, Spectrophotometric color measurement for early
549 detection and monitoring of greening on granite buildings., Biofouling. 28 (2012) 329–38.
550 doi:10.1080/08927014.2012.673220.

551 [48] P. Sanmartín, F. Villa, B. Silva, F. Cappitelli, B. Prieto, Color measurements as a reliable method for
552 estimating chlorophyll degradation to phaeopigments, Biodegradation. 22 (2011) 763–771.
553 doi:10.1007/s10532-010-9402-8.

554 [49] O. García, K. Malaga, Definition of the procedure to determine the suitability and durability of an anti-
555 graffiti product for application on cultural heritage porous materials, J. Cult. Herit. 13 (2012) 77–82.
556 doi:10.1016/j.culher.2011.07.004.

557 [50] P. Ortiz, V. Antúnez, R. Ortiz, J.M. Martín, M.A. Gómez, A.R. Hortal, B. Martínez-Haya, Comparative
558 study of pulsed laser cleaning applied to weathered marble surfaces, Appl. Surf. Sci. 283 (2013) 193–
559 201. doi:10.1016/J.APSUSC.2013.06.081.

560